Oxygen-Reduction Catalysts

DOI: 10.1002/ange.201207193

A Highly Efficient Electrocatalyst for the Oxygen Reduction Reaction: N-Doped Ketjenblack Incorporated into Fe/Fe_3C-Functionalized Melamine Foam**

Jang-Soo Lee, Gi Su Park, Sun Tai Kim, Meilin Liu, and Jaephil Cho**

Polarization caused by the oxygen reduction reaction (ORR) on cathodes still contributes significantly to the energy efficiency loss of metal–air batteries and fuel cells.[1] Thus, ways of increasing the ORR kinetics while maintaining fast mass transfer is a grand challenge in the development of a new generation of metal–air batteries and fuel cells. Catalysts based on platinum and other precious metals are very effective in facilitating the rate of ORR in batteries and fuel cells.[2] However, their high cost and low stability have hindered their practical applications in air-breathing electrodes. Accordingly, much attention has been devoted to rational design of non-precious-metal or metal-free catalysts with unique architectures to dramatically enhance ORR activity (Supporting Information, Figure S1).[3] For example, Jasinski and co-workers reported that metal/nitrogen/carbon (M/N/C) catalysts have high catalytic activity for the ORR.[4] These composite materials were synthesized by pyrolizing proper precursors with nitrogen, carbon, and abundant transition metals. While the superior catalytic activity for ORR are demonstrated,[5] there is still debate on active sites for ORR of N-M-C catalysts and their performance seems to be limited by mass transfer.[6]

To dramatically enhance mass transfer through porous oxygen-breathing electrodes, we have created some unique electrode architectures that are similar to breakwaters composed of highly porous tetrapod structures (Figure 1 a). To imitate this structure, we started with a commercially available melamine foam.[7] After pyrolysis, the open-cell network structure of the carbonized melamine foam (Supporting Information, Figure S2b) becomes very fragile, and it is easily broken to pieces by grinding with a mortar. Interestingly, the broken pieces appear similar to the tetrapod architecture (Figure 1 a). In fact, our unique electrodes consist of carbonized melamine foam and nano-sized ketjenblack, thus offering high specific surface area, large number of active sites, and large amount of pore volume for fast mass transport. Although Lin et al. used melamine resin to prepare metal-free N-doped electrocatalysts for ORR,[8] the unique architecture of carbonized melamine foam has not yet been used in synthesizing electrocatalysts for ORR (Figure 1 b).

Rotating ring–disk electrode (RRDE) experiments were used to characterize the electrocatalytic activity of the as-prepared Fe/Fe_3C-melamine/N-KB (Ar-800) (hereafter denoted as Ar-800 for brevity; Figure 2 a). First, the carbonized melamine foam showed higher positive onset potential but much lower limiting current density than pure ketjenblack

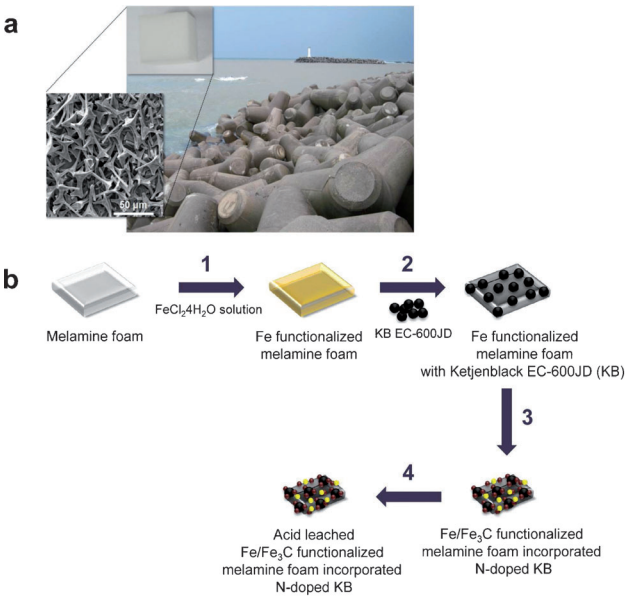

Figure 1. a) Architectural features of tetrapod structures, commercially available melamine foam (inset), and a cross-sectional view (SEM image) of a fractured melamine foam after pyrolysis. The interconnected large pores may facilitate fast mass transport. b) The synthesis of Fe/Fe_3C functionalized melamine foam infiltrated with N-doped ketjenblack (KB). 1) Impregnation of melamine foam with $FeCl_2 \cdot 4H_2O$ solution; 2) infiltration of Ketjenblack EC-600 JD; 3) carbonization in Ar atmosphere for 2 h at 800, 900, and 1000 °C; 4) leaching in a 2 M H_2SO_4 solution.

[*] J. Lee, G. Park, S. Kim, Prof. Dr. J. Cho
Interdisciplinary School of Green Energy
Ulsan National Institute of Science and Technology (UNIST)
Ulsan, 689-798 (South Korea)
E-mail: jpcho@unist.ac.kr
Homepage: http://jpcho.com
Prof. Dr. M. Liu
School of Materials Science and Engineering
Georgia Institute of Technology
771 Ferst Drive, N.W. Atlanta, GA 30332-0245 (USA)
E-mail: meilin.liu@mse.gatech.edu

[**] This work was supported by the next generation secondary battery R&D program of MKE/KEIT (10042575) and the World Class University (WCU) program supported by National Research Foundation (NRF) and the Ministry of Education, Science and Technology (MEST) of Korea.

Supporting information for this article (including the preparation of the composite Fe/Fe_3C-melamine/N-KB catalysts and details of methods, RRDE experiments, and the Zn–air full cell assembly) is available on the WWW under http://dx.doi.org/10.1002/anie.201207193.

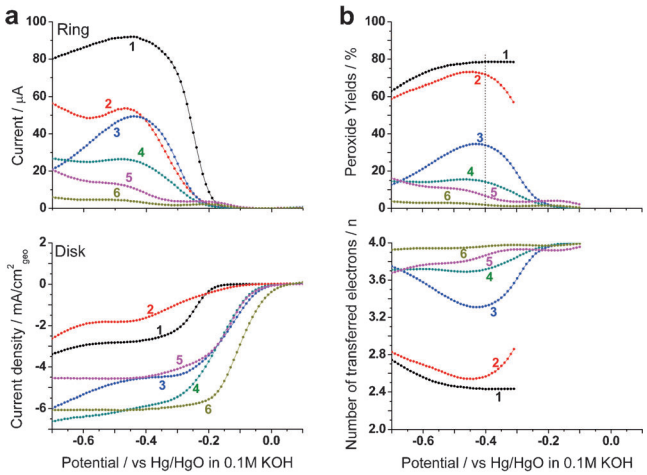

Figure 2. a) Steady-state RRDE experiments of 1) ketjenblack EC-600JD, 2) carbonized melamine foam, 3) a physical mixture of Fe/Fe_3C-melamine and KB, 4) Fe/Fe_3C-melamine/N-KB composite catalyst, 5) 9.55 $\mu g_{Pt}\,cm^{-2}$, and 6) 28.6 $\mu g_{Pt}\,cm^{-2}$ in O_2-saturated 0.1 M KOH at 2000 rpm. Non-precious-metal catalyst loadings were 0.286 $mg_{cat}\,cm^{-2}$. Ring (top) and disk current density (bottom) were separated for convenience. b) Peroxide yields (%, top) and the number of electrons (n) transferred (bottom) of as-prepared samples.

EC-600JD (KB). This result clearly indicates the importance of C–N group on the increased activity for ORR. However, carbonized melamine foam itself is ineffective because it has a very low surface area.[9] To confirm the nitrogen doping effect on the activity for the ORR, we carefully separated N-doped carbon from the Ar-800 sample and performed XPS analysis. The N 1s peaks confirmed that nitrogen was doped on KB, which had more positive onset potential and much higher current density than ketjenblack (Supporting Information, Figure S3). As melamine foam contains a large amount of nitrogen, its carbonization yields only 10 to 15 wt% of carbon at 800 °C (which is due to vaporization of unstable species and release of carbon nitride gases). To make better use of the carbon–nitrogen (C-N) content of melamine foam, commercial ketjenblack carbon was infiltrated into porous melamine foam. The micropores of the ketjenblack carbon could capture carbon nitride gases (for example, $C_2N_2^+$, $C_3N_2^+$, $C_3N_3^+$) during pyrolysis to form C–N moieties.

Apparently, the large surface area of ketjenblack enhanced limiting current density. In the case of Ar-800, dramatic shift to positive direction of its onset potential and much higher limiting current density were observed. To confirm this synergic effect between iron carbide functionalized melamine foam and N-doped ketjenblack, we further examined two different samples, a composite electrode and an electrode consisting of physical mixture of the two phases. Although the two electrode samples had very similar onset potentials, the composite electrode displayed much higher current density than the one of physical mixture, more so at higher cathodic polarization (> -0.25 V). Also, different current–voltage relationships were observed for the two electrodes at around -0.4 V. The current density of the physical mixture electrode showed a plateau at a voltage range from -0.3 V to -0.45 V and then resumed a small increase beyond -0.45 V. In contrast, the composite electrode displayed a continuous increase in current density in the entire voltage range studied, suggesting that the physical mixture had inferior performance to that of the composite electrode. As the plateau current region is very similar to that for the pure Ketjenblack electrode, the limiting current in the medium potential range is attributed to the physical portion of the ketjenblack in the mixture sample. Thus, it is reasonable to conclude that there are two types of active sites: the iron carbide functionalized melamine skeleton and the nitrogen-doped ketjenblack. Proper combination of the two, as seen in the composite electrode, has a significant synergic effect on enhancing ORR activity.

To our surprise, the current density of the as-prepared sample are even slightly higher than that for Pt/C catalysts at high overpotentials, implying that the electrode architecture of our as-prepared sample is more effective in facilitating oxygen transport to the active sites for ORR than the Pt/C catalysts under the testing conditions (Supporting Information, Table S1). Furthermore, the superior catalytic activity of the composite (Ar-800) over that of the physical mixture sample was also confirmed by the H_2O_2 yields and the number of electrons (n) transferred in the electrode reaction, as determined from the linear polarization curves (Figure 2b). In particular, the number of electrons transferred was determined to be about 3.7 to about 3.85 (very close to 4) for our best catalysts (Ar-800), suggesting that it is an efficient four-electron transfer pathway with peroxide yield of about 15% at -0.4 V. These results indicate that the composite samples are very promising electrocatalysts for the ORR in an alkaline solution, demonstrating highly competitive performance but at a much lower cost than the benchmarked Pt/C catalysts.

For practical applications, resistance to the methanol crossover effect and durability of the catalysts are important considerations as well. The chronoamperometric response of the Ar-800 sample recovered quickly, about 150 s after methanol injection (Figure 3a), meaning that the catalyst was not influenced by methanol crossover.

In contrast, the chronoamperometric response of the Pt/C catalyst changed dramatically after methanol injection (Figure 3a), suggesting that the methanol oxidation reaction (MOR) initiated, because the sign of current changed from

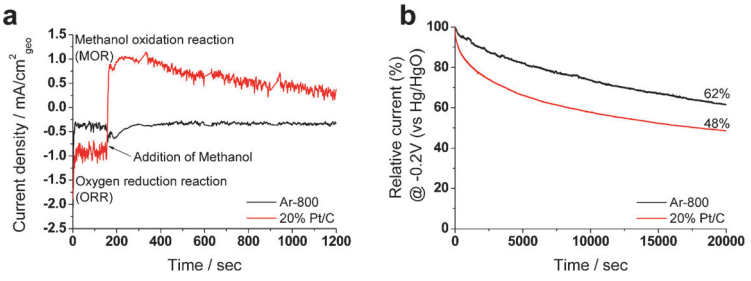

Figure 3. a) Chronoamperometric response with 10% (w/w) methanol; b) chronoamperometric response of Ar-800 and 20% Pt/C in O_2-saturated 0.1 M KOH solution at -0.2 V (vs Hg/HgO) and 1600 rpm.

negative for the ORR to positive for the MOR. It clearly demonstrated that our catalyst has superior tolerance against methanol crossover effect. Further, the time-dependence data of performance suggested that the Ar-800 catalyst degraded in a slower rate than the Pt/C catalysts (Figure 3b). This result implies that our catalysts are promising candidates for direct methanol and alkaline fuel cells as well.

We also constructed Zn-air full cells using our catalysts and the Pt/C catalysts. Performance evaluation of these cells (Figure 4a) indicates that, at low current densities, there is a gap in power output between Ar-800 and Pt/C catalysts, which is consistent with the observations with the half cells discussed earlier. At higher current densities, however, the voltage of our catalysts became higher than that of the cell with Pt/C catalysts; the corresponding peak power density of the cell with our catalyst was about 200 mW cm^{-2}, which is slightly higher than about 195 mW cm^{-2} for the cell with the Pt/C catalyst (Figure 4b). These measurements are consistent with the RRDE results (Figure 2a), suggesting that our catalysts have unique porous architecture for rapid mass and charge transfer.

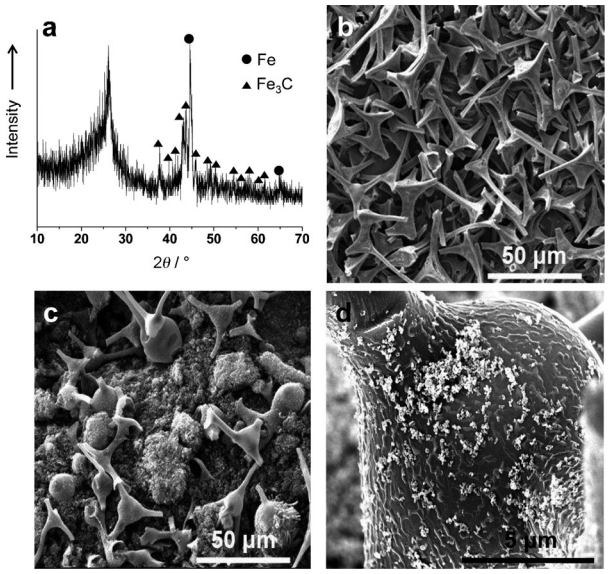

Figure 5. a) X-ray diffraction patterns of Ar-800. b) A SEM image of ground melamine foam structures after carbonization, c) an SEM image of Ar-800, and d) a higher magnification of the image of (c).

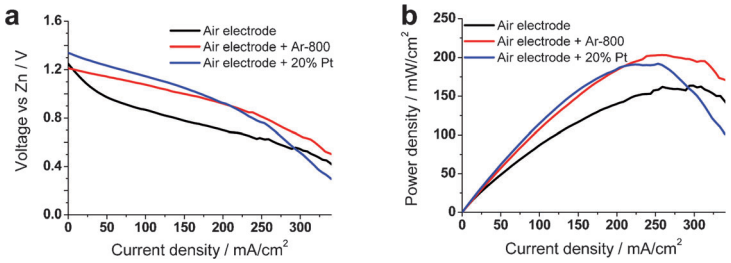

Figure 4. a) Current–voltage and b) power–voltage curves of Zn–air cells with Ar-800 and 20% Pt/C catalysts. A gas diffusion layer without any catalysts was used as the baseline air electrode for comparison.

To correlate the high performance with the microscopic features of the as-prepared samples, we examined the crystalline phases of Ar-800. XRD analyses (Figure 5a) indicate that metallic Fe, Fe_3C, and graphitic carbon co-existed, according to the diffraction data for α-Fe (JCPDS No. 87-0722) and Fe_3C (JCPDS No. 89-2867).[6,10] Other samples heat treated at higher temperatures (900 and 1000 °C) for 2 h also showed the same diffraction patterns (Supporting Information, Figure S4a). However, the intensities of the peaks related to iron species were low owing to low iron content (ca. 3.30 wt %) in the Ar-800 sample (Supporting Information, Figure S5).

At low magnification, the morphological features of the Ar-800 (Figure 5c) appear similar to those of the melamine foam (Figure 5b); at higher magnification, however, Fe/Fe_3C nanorods and ketjenblack carbon are evenly attached onto the surface of melamine foam in Ar-800 (Figure 5d; Supporting Information, Figure S6a,b). The nanorods have a diameter of about 100 nm with a length of around 0.6 to 1 μm. The well-defined crystalline phase has a lattice fringe with d spacing of 0.184 nm, which is consistent with the (221) plane of Fe_3C (Supporting Information, Figure S6b,d).

To examine the effect of pyrolysis temperature on catalytic activity for the ORR, the samples were pyrolyzed under Ar atmosphere at 800, 900, and 1000 °C. Linear-sweep voltammetry curves (Figure 6a) for the three samples (Ar-800, 900, and 1000) indicate that Ar-800 had more positive onset potential and higher current density than the other two samples pyrolyzed at higher temperatures. To gain more insight into the surface properties of the catalysts, we performed XPS analysis of the samples. High-resolution XPS spectra suggest that with increasing pyrolysis temperature, the amount of pyridinic moiety decreased but quaternary nitrogen increased (Figure 6c). Thus, proper combination of pyridinic N and pyrrolic N could be a key factor affecting the enhanced catalytic activity for ORR. This conclusion seems to contradict a previous report that graphite-like nitrogen atoms are more important in metal-free catalysts.[11] In our case, the iron precursor may be easily bounded to (and stabilized with) the nitrogen atom with lone pair electrons for further growth of Fe/Fe_3C particles. Therefore, our conclusion seems to be reasonable. On the other hand, sulfur was not affected by the heat-treatment temperature (Figure 6d), implying that sulfur may not significantly affect the catalytic activity for ORR. One possible explanation is that sulfur exists as bisulfite in pristine melamine structure, not in the C-N skeleton of melamine. XPS analyses support our hypothesis. Sulfur is found to be in the form of −C−SO_x−C−, not in the form of −C−S−C−.[12]

However, it is worth noting that the −C−SO_x−C− moiety may increase the hydrophilicity of carbon plane so that more electrolyte (together with dissolved oxygen) may gain easy access to the catalytic active sites. Meanwhile, oxygen gas may move along hydrophobic moiety. Therefore, proper combination of hydrophobic and hydrophilic property in catalyst

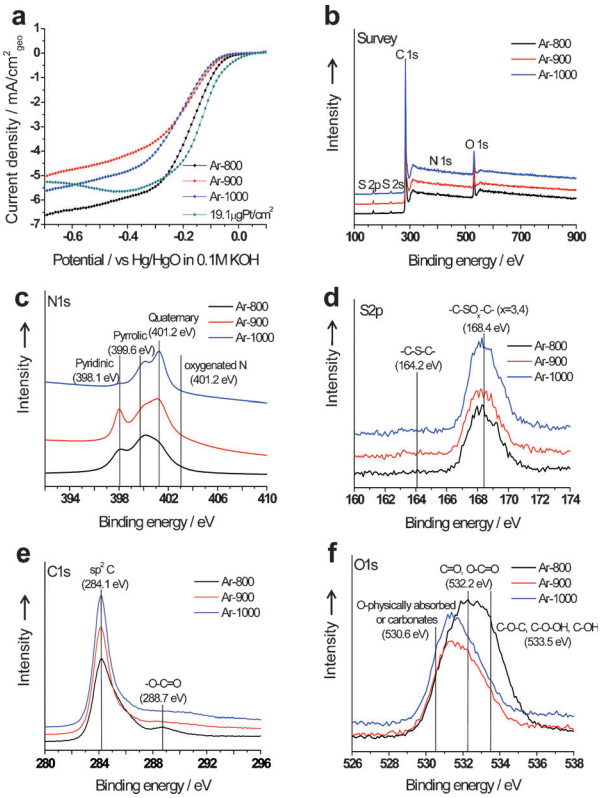

Figure 6. a) Steady-state LSV curves of composite Fe/Fe_3C-melamine/N-KB samples pyrolyzed at different temperatures: 800 °C (Ar-800), 900 °C (Ar-900), and 1000 °C (Ar-1000), as compared to that for 19.1 $\mu g_{Pt}\,cm^{-2}$ catalyst. b) XPS survey and high resolution c) N 1s, d) S 2p, e) C 1s, and f) O 1s spectra of as-prepared samples.

design is vital to facilitating fast transport of reactants for ORR. Another origin of hydrophilicity is supported by C 1s and O 1s spectra. For the C 1s spectra, as expected, the center peak of sp^2 C around 284.1 eV became more symmetric as the heating temperature increased, implying that the degree of graphitization of the as-prepared samples increased with temperature (Figure 6e). This result is also supported by XRD and Raman data (Supporting Information, Figure S4). Obviously, graphitization could affect catalytic activity for ORR owing to increased electrical conductivity and improved hydrophobicity. Further, the −O−C=O group was still present in Ar-800, which may increase the hydrophilicity of the sample and its affinity to aqueous electrolyte (Figure 6f).

XPS analysis of the iron species was less successful; it was almost impossible to determine the exact oxidation state of Fe (Fe 2p, 702–740 eV), which is due to very week signal intensity (Figure 6b; Supporting Information, Table S2).[13] XRD analysis indicates, however, that most iron species exist as metallic Fe or iron carbide (Fe_3C), not iron oxide. Furthermore, iron oxides (Fe_2O_3, Fe_3O_4) are hardly detected at 529.5 eV[14] in the O 1s spectra. Also, no peaks related to the redox $Fe^{II}/^{III}$couple are observable in the ORR region of cyclic voltammetry curves, even at very high scan rates (Supporting Information, Figure S7).[15] Accordingly, it is reasonable to conclude that iron redox couple ($Fe^{II}/^{III}$) might not play an important role in the ORR.

In conclusion, nanosized ketjenblack clusters were successfully incorporated into commercially available melamine foam of microscale porous skeleton through a simple solution based method and pyrolysis, creating unique catalyst architectures with a large number of active sites for the ORR and large pore volume for fast transport of oxygen gas and aqueous electrolyte to the active sites. Electrochemical performances of the low-cost catalysts are comparable to those of Pt-based catalysts at low overpotentials and even better at high overpotentials. XPS analysis suggests that −C−SO_x−C, C=O, and C−OH in the as-prepared sample may increase hydrophilicity, thus enhancing transport through the porous catalysts. Performance measurements using RRDE and Zn–air cells suggest that a large surface area of N-doped ketjenblack and Fe/Fe_3C of melamine carbon foam are responsible for the dramatically increased ORR activity. Good methanol tolerant and durability were also demonstrated. As commercially available melamine foam and ketjenblack carbon are relatively inexpensive and the facile synthetic method is amendable to mass production, the non-precious metal catalysts are a promising alternative for a new generation of low-cost and high-performance metal–air batteries and fuel cells.

Received: September 5, 2012
Revised: October 29, 2012
Published online: November 28, 2012

Keywords: electrocatalysts · ketjenblack · melamine foam · oxygen reduction reaction

[1] a) J.-S. Lee, S. Tai Kim, R. Cao, N.-S. Choi, M. Liu, K. T. Lee, J. Cho, *Adv. Energy Mater.* **2011**, *1*, 34–50; b) M. Armand, J. M. Tarascon, *Nature* **2008**, *451*, 652–657; c) P. G. Bruce, S. A. Freunberger, L. J. Hardwick, J.-M. Tarascon, *Nat. Mater.* **2012**, *11*, 19–29.

[2] a) B. Lim, M. Jiang, P. H. C. Camargo, E. C. Cho, J. Tao, X. Lu, Y. Zhu, Y. Xia, *Science* **2009**, *324*, 1302–1305; b) J. Greeley, I. E. L. Stephens, A. S. Bondarenko, T. P. Johansson, H. A. Hansen, T. F. Jaramillo, J. Rossmeisl, I. Chorkendorff, J. K. Nørskov, *Nat. Chem.* **2009**, *1*, 552–556; c) V. R. Stamenkovic, B. Fowler, B. S. Mun, G. Wang, P. N. Ross, C. A. Lucas, N. M. Markovic, *Science* **2007**, *315*, 493–497; d) H. A. Gasteiger, S. S. Kocha, B. Sompalli, F. T. Wagner, *Appl. Catal. B* **2005**, *56*, 9–35; e) E. Antolini, J. R. C. Salgado, M. J. Giz, E. R. Gonzalez, *Int. J. Hydrogen Energy* **2005**, *30*, 1213–1220.

[3] a) R. Cao, J.-S. Lee, M. Liu, J. Cho, *Adv. Energy Mater.* **2012**, *2*, 701–701; b) Z. Chen, D. Higgins, A. Yu, L. Zhang, J. Zhang, *Energy Environ. Sci.* **2011**, *4*, 3167–3192; c) F. Jaouen, E. Proietti, M. Lefevre, R. Chenitz, J.-P. Dodelet, G. Wu, H. T. Chung, C. M. Johnston, P. Zelenay, *Energy Environ. Sci.* **2011**, *4*, 114–130.

[4] a) C. W. B. Bezerra, L. Zhang, K. Lee, H. Liu, A. L. B. Marques, E. P. Marques, H. Wang, J. Zhang, *Electrochim. Acta* **2008**, *53*, 4937–4951; b) R. Jasinski, *Nature* **1964**, *201*, 1212–1213.

[5] a) G. Wu, K. L. More, C. M. Johnston, P. Zelenay, *Science* **2011**, *332*, 443–447; b) E. Proietti, F. Jaouen, M. Lefèvre, N. Larouche, J. Tian, J. Herranz, J.-P. Dodelet, *Nat. Commun.* **2011**, *2*, 416; c) M. Lefevre, E. Proietti, F. Jaouen, J. P. Dodelet, *Science* **2009**, *324*, 71–74; d) J.-Y. Choi, R. S. Hsu, Z. Chen, *J. Phys. Chem. C* **2010**, *114*, 8048–8053.

[6] Z. Wen, S. Ci, F. Zhang, X. Feng, S. Cui, S. Mao, S. Luo, Z. He, J. Chen, *Adv. Mater.* **2012**, *24*, 1399 – 1404.
[7] http://www.plasticsportal.net/wa/plasticsEU/portal/show/content/products/foams/basotect.
[8] Z. Lin, M.-K. Song, Y. Ding, Y. Liu, M. Liu, C.-P. Wong, *Phys. Chem. Chem. Phys.* **2012**, *14*, 3381 – 3387.
[9] M. Kodama, J. Yamashita, Y. Soneda, H. Hatori, K. Kamegawa, *Carbon* **2007**, *45*, 1105 – 1107.
[10] X. L. Dong, Z. D. Zhang, Q. F. Xiao, X. G. Zhao, Y. C. Chuang, S. R. Jin, W. M. Sun, Z. J. Li, Z. X. Zheng, H. Yang, *J. Mater. Sci.* **1998**, *33*, 1915 – 1919.
[11] R. Liu, D. Wu, X. Feng, K. Müllen, *Angew. Chem.* **2010**, *122*, 2619 – 2623; *Angew. Chem. Int. Ed.* **2010**, *49*, 2565 – 2569.
[12] a) Z. Yang, Z. Yao, G. Li, G. Fang, H. Nie, Z. Liu, X. Zhou, X. a. Chen, S. Huang, *ACS Nano* **2012**, *6*, 205 – 211; b) C. H. Choi, S. H. Park, S. I. Woo, *Green Chem.* **2011**, *13*, 406 – 412; c) Y. P. Wu, S. Fang, Y. Jiang, R. Holze, *J. Power Sources* **2002**, *108*, 245 – 249.
[13] H. R. Byon, J. Suntivich, Y. Shao-Horn, *Chem. Mater.* **2011**, *23*, 3421 – 3428.
[14] V. Datsyuk, M. Kalyva, K. Papagelis, J. Parthenios, D. Tasis, A. Siokou, I. Kallitsis, C. Galiotis, *Carbon* **2008**, *46*, 833 – 840.
[15] L. Zhang, K. Lee, C. W. B. Bezerra, J. Zhang, J. Zhang, *Electrochim. Acta* **2009**, *54*, 6631 – 6636.